ELSEVIER

Cement & Concrete Composites 24 (2002) 361–370

Cement & Concrete Composites

www.elsevier.com/locate/cemconcomp

Ettringite and thaumasite formation in laboratory concretes prepared using sulfate-resisting cements

Paul Brown [a,*], R.D. Hooton [b]

[a] Department of Materials Science and Engineering, The Pennsylvania State University, University Park, PA 16802, USA
[b] The University of Toronto, Toronto, Canada

Abstract

Four series of micrographs are presented illustrating the microstructures resulting from the long-term immersion (21 years) in sulfate solutions of concretes prepared using either a Type II or a Type V Portland cement. The effects of cement type (II or V), water-to-cement ratio (0.45 or 0.50) and the sulfate solution (Na_2SO_4 or $MgSO_4$) on microstructural evolution were analyzed. Gradients were observed in sulfate-containing solids from the concrete surfaces inward. Such gradients are consistent with immersion in sulfate solutions in that the extent of sulfate attack was progressively diminished at locations increasingly remote from the surfaces. Although the samples were stored at ambient temperatures, extensive thaumasite formation was observed. © 2002 Published by Elsevier Science Ltd.

Keywords: Sulfate; Thaumasite; Concretes

1. Introduction

Sulfate attack of concrete is a well-recognized phenomenon and a large body of literature has been directed towards this topic e.g., [1–4]. Recently, a distinction has been made regarding "internal" and "external" sulfate attack. In internal sulfate attack, the constituents necessary for deleterious expansion and cracking to occur are present in the concrete at the time of placement. This form of sulfate attack is primarily associated with concretes subjected to heat treatment. In external sulfate attack, one or more of the species that participates in the attack is derived from an external source. Most typically, external sources include natural waters. The severity of sulfate attack may also be related to the cation associated with the sulfate anion. The solubility of calcium sulfate is about 2000 ppm, whereas those of sodium sulfate and magnesium sulfate are much higher. If the associated cation is magnesium, it can participate in the reactions as a consequence of brucite or magnesium silicate formation. The effects of both sodium and magnesium sulfate were explored in the present study.

Various organizations recognize that the extent of sulfate attack can be limited by a combination of compositional control and permeability control. This recognition has led to limits on the C_3A contents of cements to be used in applications where sulfate resistance is a consideration by ASTM specification C-150 [5]. Codes for practitioners, such as the Uniform Building Code, have placed limits on the water-to-cement (w/c) ratios of concretes used in these applications. A large number of studies have been carried to demonstrate the importance of both these limitations. Fewer long-term studies have been done. Notable among these is the study carried out the PCA at an exposure site in Northern California [6, and references cited]. Herein, we report the results of a long-term study that evaluates the responses of laboratory concretes to sulfate attack. This study illustrates the importance of both cement type and w/c ratio in conferring a concrete the ability to resist sulfate attack.

Among the compounds formed as a result of sulfate attack are ettringite, gypsum, and thaumasite. Thaumasite formation was first identified in deteriorated concrete in 1965 [7]. Thaumasite formation is generally associated with concretes exposed to carbonate and sulfate at low temperatures [8,9]. Recent examinations of field concrete have shown that thaumasite can be formed in field concrete placed in a warm climate [10].

* Corresponding author.
E-mail address: etx@psu.edu (P. Brown).

0958-9465/02/$ - see front matter © 2002 Published by Elsevier Science Ltd.
PII: S0958-9465(01)00088-9

The present study confirms this finding for laboratory concretes.

2. Experimental program

The concrete samples examined in this study were prepared in April 1977 as control samples in a study on the sulfate resistance of slag cements. The ASTM Type V sulfate-resistant cement used contained 3.5% C_3A while the C_3A content of the ASTM Type II moderate-sulfate resistant cement was 7.1%. The concretes were air-entrained and 20 mm crushed glacial gravel of mixed siliceous and carbonate content was used. Commercial ready mixed concretes supplied in 6 m^3 batches were used to prepare numerous concrete cylinders 75×150 mm^2 . These were cast at room temperature. Molds were stripped after 48 h and the concretes were stored in water at 23 °C until compressive strengths of between 29.7 and 33.1 MPa were attained for the concretes studied in this paper. Subsequently, the cylinders were stored in 1000, 2000, or 3000 ppm SO_4 (as Na_2SO_4) solutions or in 3000 ppm SO_4 (as $MgSO_4$) solution. Further details regarding cement compositions and mix designs have been published elsewhere by Hooton and Emery [11]. Various concrete properties were monitored every 3 months for 4 years. The concretes were then stored in a laboratory warehouse (This warehouse was not temperature controlled but the building was heated during winter. The estimated temperature range is 23 ± 7 °C.) until an age of 8 years when they were visually inspected. At this time it was decided to increase the sulfate exposure concentrations to accelerate thee attack. All the Na_2SO_4 exposed cylinders were immersed in 50,000 ppm SO_4 (as (Na_2SO_4) and the $MgSO_4$ exposed cylinders in 50,000 ppm SO_4 (as $MgSO_4$). Subsequent to this, they were again stored for three more years in the warehouse and then transferred to a 23 °C laboratory until they were obtained for the present study at an age of 21 years.

Samples were sliced from the cylinders using a diamond wheel saw in preparation of SEM analyses. These were then epoxy impregnated, polished, and carbon coated. SEM/EDX analyses were carried out on polished sections.

3. Results and discussion

3.1. Concrete containing Type V cement, $w/c = 0.45$, immersed in Na_2SO_4 solution

Fig. 1 shows a microstructure typical of an unattacked region approximately 22 mm below the surface of the concrete. The microstructure is characterized by numerous air voids that are clean or only partially

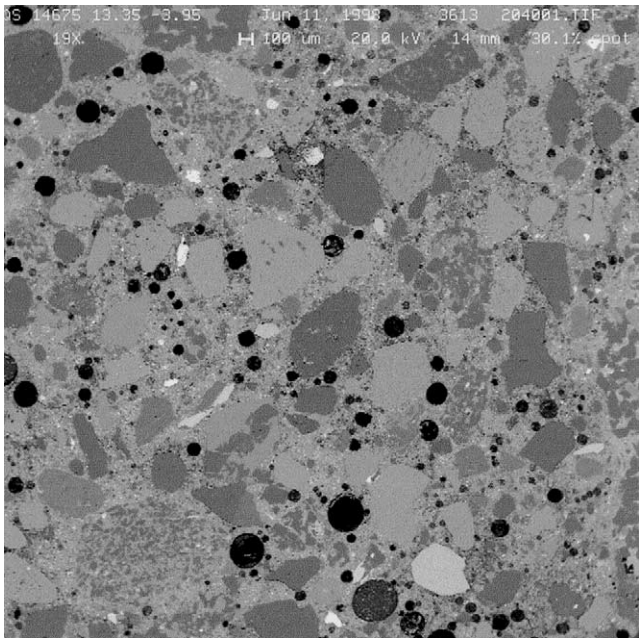

Fig. 1. Air void structure in a Type V cement concrete; w/c = 0.45; percent air = 5.5. Some air voids are clean and others are partially filled. The air void near the bottom center of the micrograph appears to be completely filled. The paste is well bonded to the aggregate and cracks are not apparent at this magnification (19×).

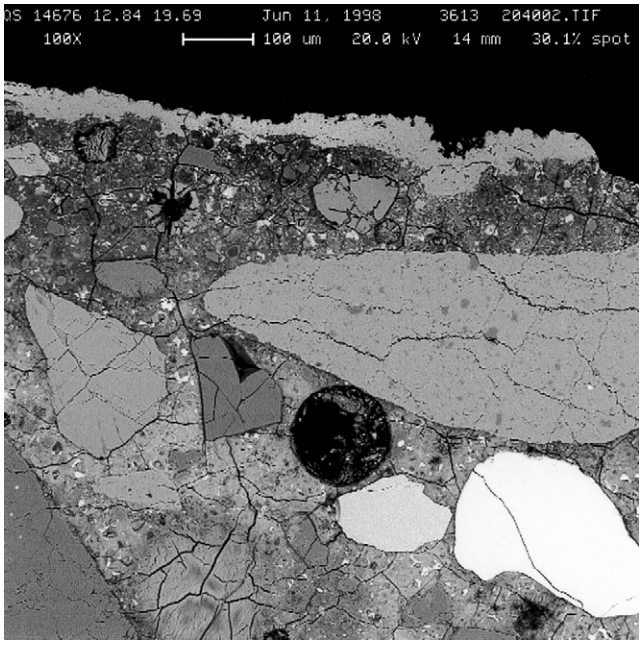

Fig. 2. The near-surface microstructure of a w/c = 0.45 Type V cement concrete after immersion in Na_2SO_4 solution for 22 years. A thin (~50 μm) carbonate layer can be observed. Air voids are partially or completely filled and a network of cracks is apparent. As can be observed by comparing the air voids two, distinct morphologies can be observed.

filled. The paste is well bonded to the aggregate and there is no evidence of cracking.

Fig. 2 shows the near-surface region of the specimen. The immediate surface shows a thin layer has deposited. An EDS spectrum indicated this layer to be $CaCO_3$. Air voids partially filled with ettringite can be seen immediately below the exposed surface (~100 μm). This observation is consistent with the formation of ettringite due to the ingress of sulfate from the storage solution. Fig. 3 confirms the presence of ettringite in this region. The tiger stripe morphology observed is typical of ettringite and the related EDS spectrum indicates the relative Al, S and Ca peak intensities expected for ettringite. As this figure shows, this void is entirely filled and cracks radiate from it.

Fig. 4 shows another void in this near-surface region to be filled with a solid having a morphology similar to that of ettringite, but not identical. The EDS spectrum for this solid indicates it to be thaumasite. The relative intensities of the Si, S and Ca peaks in the spectrum shown are typical of thaumasite. As with the ettringite-filled void, cracks radiate from the thaumasite-filled void as well. In both instances, the cracks form a network with a mesh size approximating that of the fine aggregate.

Fig. 5 shows the ettringite reaction zone has extended to approximately 20 mm below the surface as indicated by ettringite in the paste and partially filling the air voids. However, clean air voids can be observed in this micrograph as well and much less cracking is observed. Thus, these data indicate the alumina content of the Type V cement used ($C_3A = 3.5\%$) in this concrete was

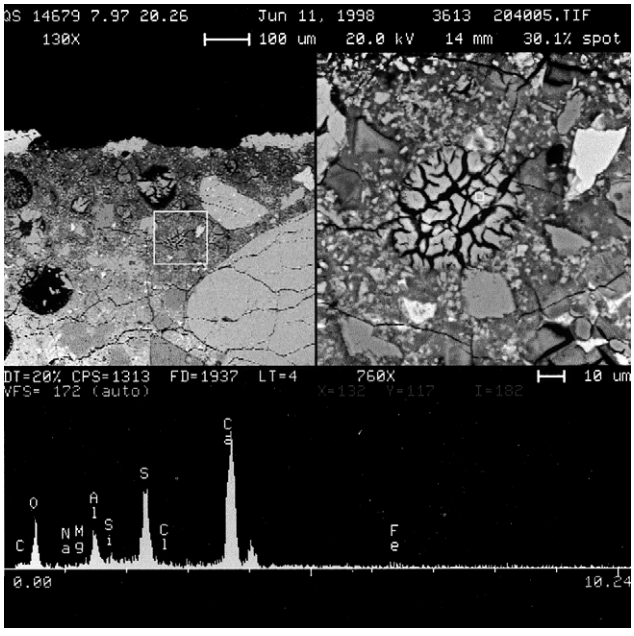

Fig. 3. An ettringite-filled air void. The tiger stripe morphology is typical of ettringite and the EDS spectrum for the region associated with the small box on the right image shows the Al, S, and Ca peak heights expected for ettringite. Cracks radiating from the ettringite propagate through the paste.

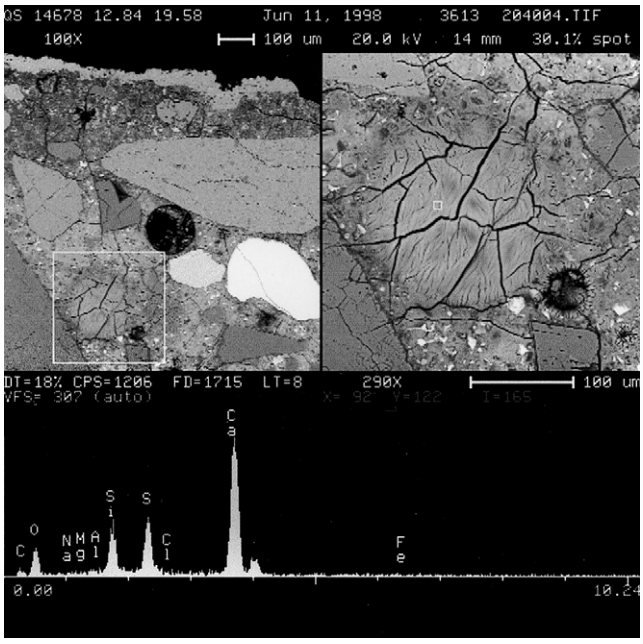

Fig. 4. An air void filled with thaumasite. The fibrous morphology of thaumasite can be discerned. The EDS spectrum shows peaks for Si, S, and Ca. An Al peak is not observed. The Si, S, and Ca peak heights are those that would be expected for thaumasite. Cracks radiate from the thaumasite deposit into the paste.

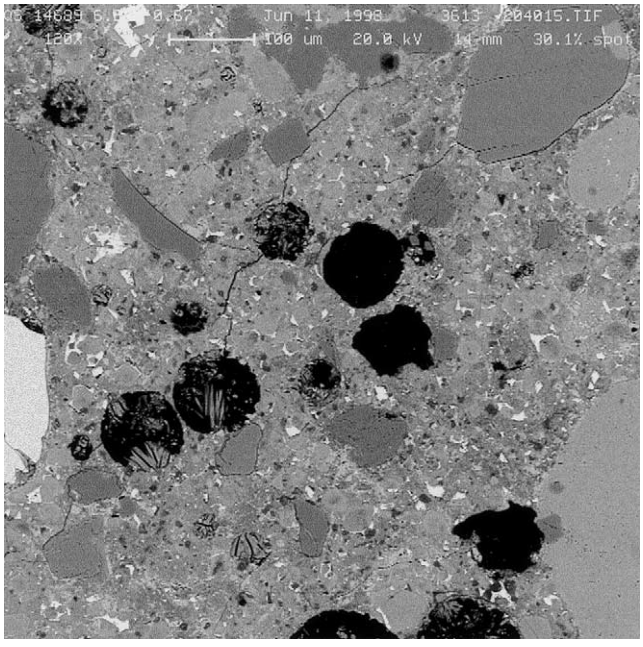

Fig. 5. Ettringite partially filling an air void in the paste about 20 mm below the surface. While cracks can still be observed at this depth, their density is much reduced.

sufficient to permit formation of substantial ettringite. While the C_3A contents of Type V and in Type I cements can differ substantially, e.g., 4% C_3A vs. ~12% C_3A, the total alumina contents of Type V cements are only about 1/3 less than those of Type I cements. Thus, both cement types show the potential of forming significant ettringite. The present microstructural data show that ettringite formed in sufficient quantity in a concrete produced with a Type V cement to result in the physical damage to the specimen. The comparison of Figs. 1 and 2 suggests some depletion of the ferrite phase ($C_4AF = 13.2\%$) in the near-surface region. The presence of the high atomic number ferrite phase is evident in Fig. 1 at low magnification as the bright features throughout the micrograph. Compared to this, the ferrite phase appears to be depleted in the near-surface regions, as illustrated in Fig. 2. Thus, the possibility of alumina originally present in C_3A and in C_4AF participating in ettringite formation cannot be precluded.

These data show that attack is more than surfacial having proceeded to a depth of about 22 mm in 21 years. The expansive reactions associated with ettringite formation and, possibly, with thaumasite formation create crack networks permitting the ingress of additional sulfate and carbonate or bicarbonate ions. In this event the rate of ingress is no longer dependent on diffusionally controlled processes.

3.2. Concrete containing Type V cement, $w/c = 0.45$, immersed in $MgSO_4$ solution

Fig. 6 shows the near-surface region of concrete containing Type V cement and produced at $w/c = 0.45$ after immersion in $MgSO_4$ solution. As has been variously reported, a layer of brucite several hundred micrometers in thickness had developed [12,13]. The precipitation of brucite layers has been reported to decrease the surface permeability of concrete thereby rendering it less susceptible to further attack. Present findings support this view. The extent of cracking due to sulfate attack in this specimen appears to be limited to a layer approximately 7 mm in thickness. Thus, the extent of the damaged zone in this concrete is only about one third of that after immersion in a comparable concentration of Na_2SO_4. Magnesium silicate formation accompanies that of brucite in this near-surface region. Fig. 7 shows a region where magnesium silicate has formed. Similar observations have been made on pastes produced in the laboratory [14] and on field concretes that were subjected to mixed magnesium sulfate/sodium sulfate attack while in service [10]. The magnesium cation tends to precipitate as its hydroxide at high pH values. One consequence of this is that magnesium sulfate will participate in base exchange reactions in concrete. The reaction involving calcium hydroxide

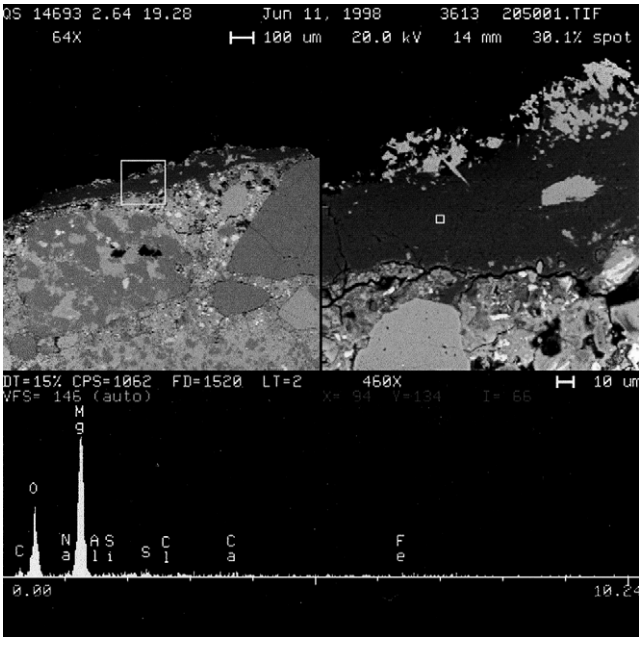

Fig. 6. The presence of a brucite layer on the surface of a $w/c = 0.45$ Type V cement concrete after immersion in $MgSO_4$ solution. The continuity of this layer is consistent with it serving a barrier function.

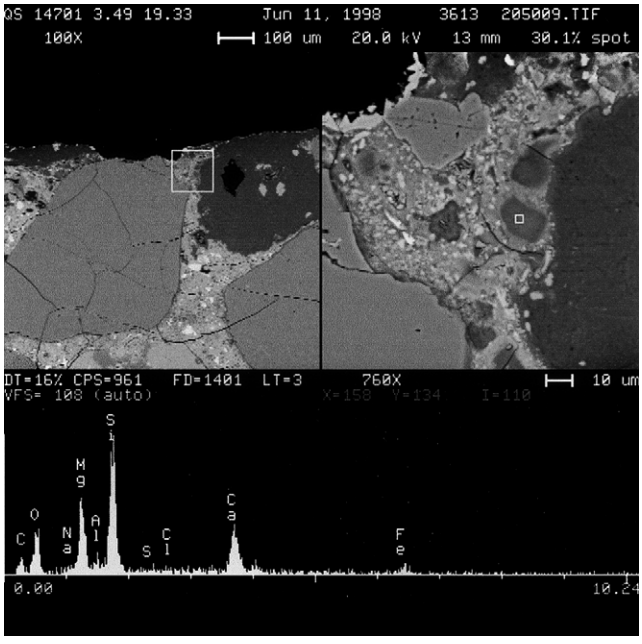

Fig. 7. A Mg-rich region. It cannot be determined whether this is a magnesium silicate compound or a intimate mixture of brucite and hydrous silica. Magnesium compounds have been observed to form either by the reaction of Mg with $Ca(OH)_2$, with C–S–H or with anhydrous calcium silicates.

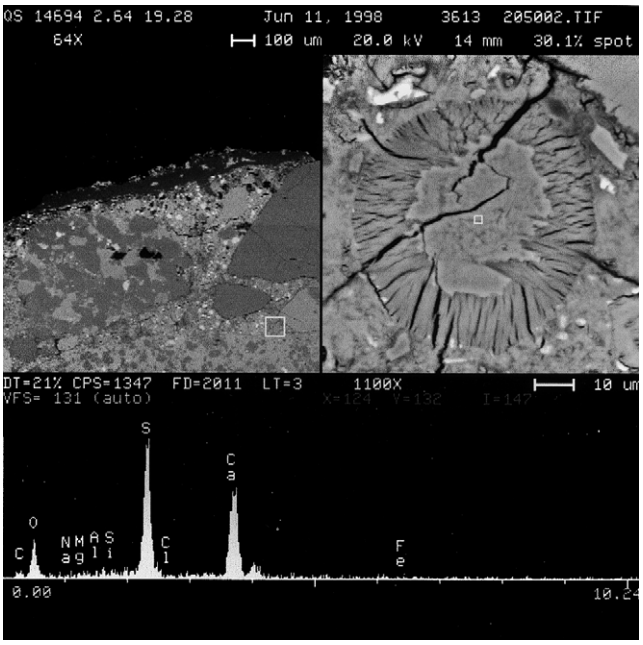

Fig. 8. An air void filled with solids having distinct morphologies. The inner-most solid is structureless and its EDS spectrum reveals this solid to be gypsum.

$$MgSO_4 + Ca(OH)_2 \rightarrow CaSO_4 \cdot 2H_2O + Mg(OH)_2$$

and brucite is produced.

The reaction involving C–S–H is

$$1.7MgSO_{4(aq)} + 1.7CaO{\cdot}SiO_2 \cdot 4H_2O \rightarrow 1.7CaSO_4 \cdot 2H_2O + xSiO_2 \cdot yMgO \cdot zH_2O$$

One product of this reaction is either a physical mixture of brucite and hydrous silica or a magnesium silicate hydrate. As Figs. 6 and 7 show, both reactions have occurred in this concrete. Also indicative of the occurrence of these reaction is the precipitation of gypsum, as is illustrated in Fig. 8. A gypsum core can be seen in the center of a small pore or void. Surrounding the gypsum core is a shell of thaumasite, Fig. 9. This spatial relationship between thaumasite and gypsum is consistent with the conversion of the gypsum and hydrous silica and calcium carbonate from the carbonated and decalcified paste in this near-surface region to thaumasite.

Filled air voids were typically observed in the regions of these concrete specimens where sulfate attack is occurring. Most typically, the air voids are filled with ettringite, with thaumasite or with a mixture of the two. Although cracking was primarily confined to a layer about 7 mm thick, ettringite formation is occurring more deeply below the surface. Fig. 10 shows a filled air void about 16 mm below the surface. The EDS spectrum in this figure confirms the presence of ettringite. Fig. 11 indicates calcium hydroxide is also present. This assemblage of compounds is consistent with the ingress

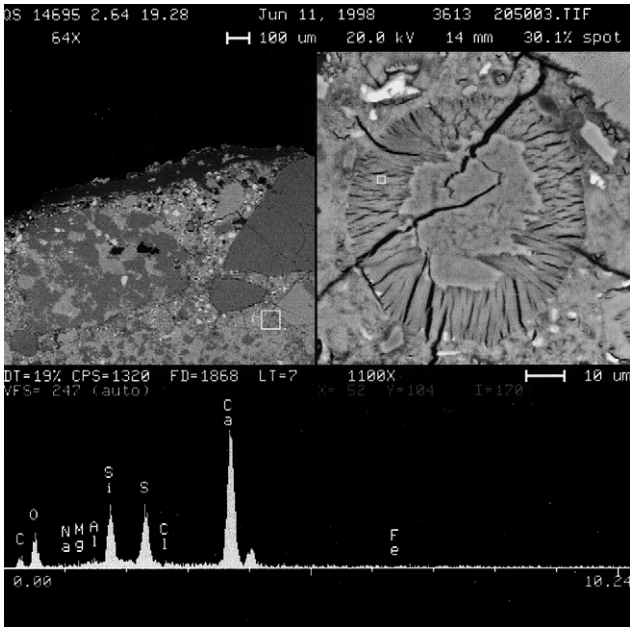

Fig. 9. The same filled air void as shown in Fig. 8. The EDS spectrum of the fibrous solid surrounding the gypsum indicates it to be thaumasite.

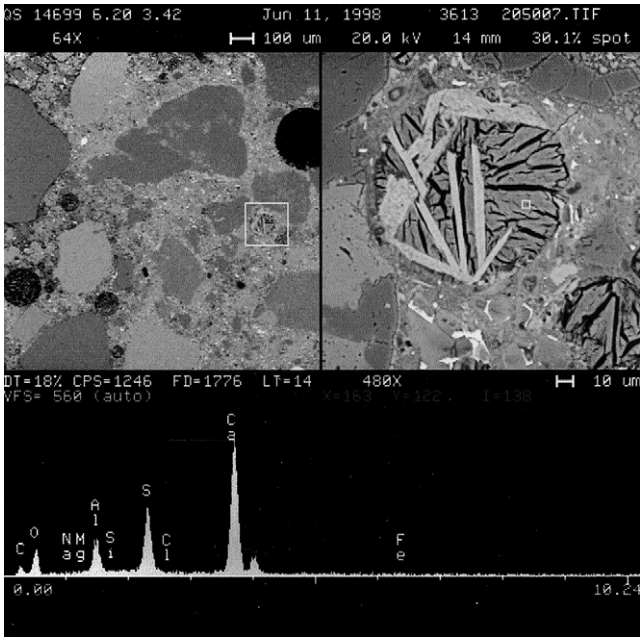

Fig. 10. An air void filled with solids having morphologies distinct from each other and distinct from those shown in Figs. 8 and 9. A solid with an ettringite-like morphology is present and the EDS spectrum confirms the presence of ettringite.

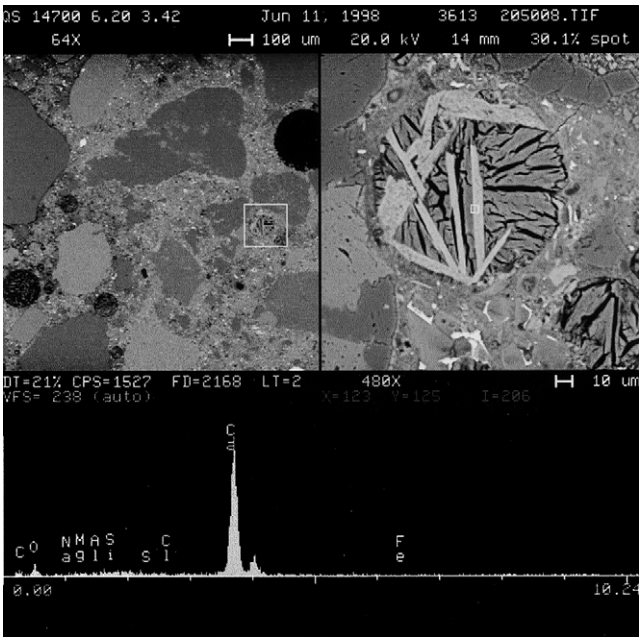

Fig. 11. The same air void as shown in Fig. 10. The EDS spectrum of the needle-like feature indicates it to be $Ca(OH)_2$.

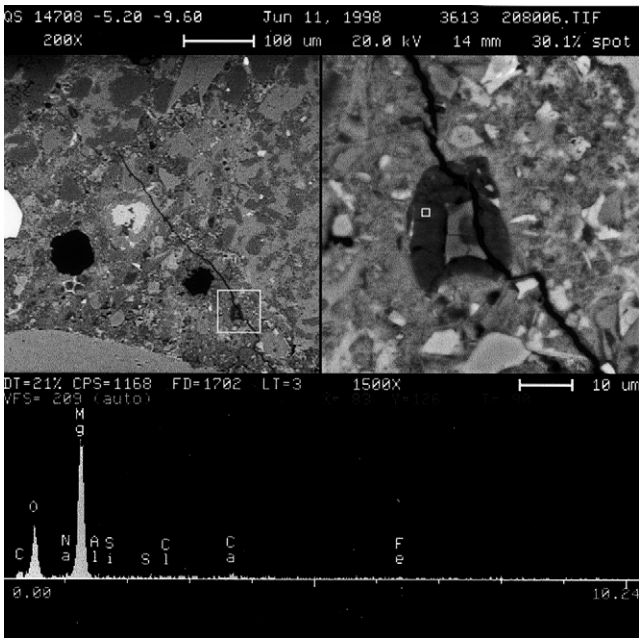

Fig. 13. An EDS spectrum from the dark region surrounding the periclase particle. This spectrum indicates this region to be brucite thus indicating the slow hydration of MgO during the extended period of immersion.

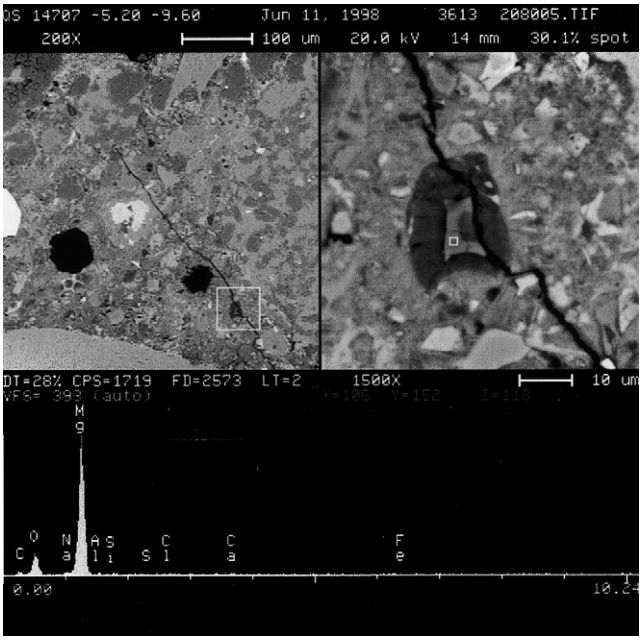

Fig. 12. A particle surrounded by a darker region. The EDS spectrum indicates the particle to be periclase.

of sulfate followed by its reaction to form ettringite at locations where $Ca(OH)_2$ is available.

The microstructural data presented illustrate that the selection of Type V cement alone does not confer immunity to sulfate attack or to thaumasite formation. Alternatively, the use a low w/c ratio limits the extent of sulfate attack provided that cracking does not occur.

3.3. Concrete containing Type II cement, $w/c = 0.5$, immersed in $MgSO_4$ solution

Compared to that of the Type V concrete immersed in $MgSO_4$ solution, generally similar microstructural evolution occurs when concrete produced at $w/c = 0.5$ using Type II cement is immersed in $MgSO_4$ solution. The air void structure at a depth of ~32 mm from the surface was ettringite filled, whereas the air void structure at a depth of ~35 mm below the surface was clean. Compared to the depths of ettringite formation described above, increasing the w/c by a value of 0.05 increased the depth of attack by about 25 mm. Thus, the depth of attack has increased significantly compared to that in the concrete prepared at w/c 0.45. The role of Mg is also evident in the analysis of this concrete. However, it cannot be assumed that all the Mg observed in the concrete entered from the external source. For example Fig. 12 shows a particle that contains only Mg (Ca, Si, Al, and Fe are absent). Fig. 13 shows the region surrounding this particle also to contain only Mg. The relative heights of the oxygen peaks suggest the former to be a periclase grain and the latter to be brucite that formed from this periclase over the period of immersion. Alternatively, the Mg-rich

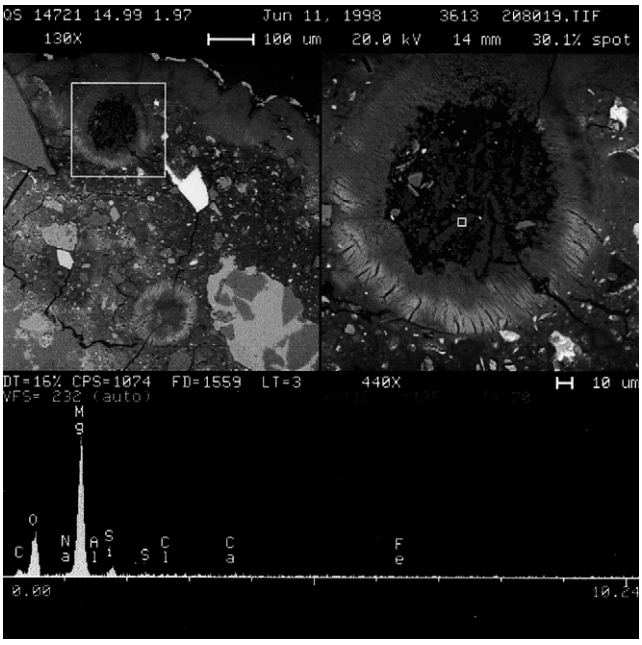

Fig. 14. A brucite deposit that has accumulated at the core of an air void. Surrounding this core is a layer of thaumasite.

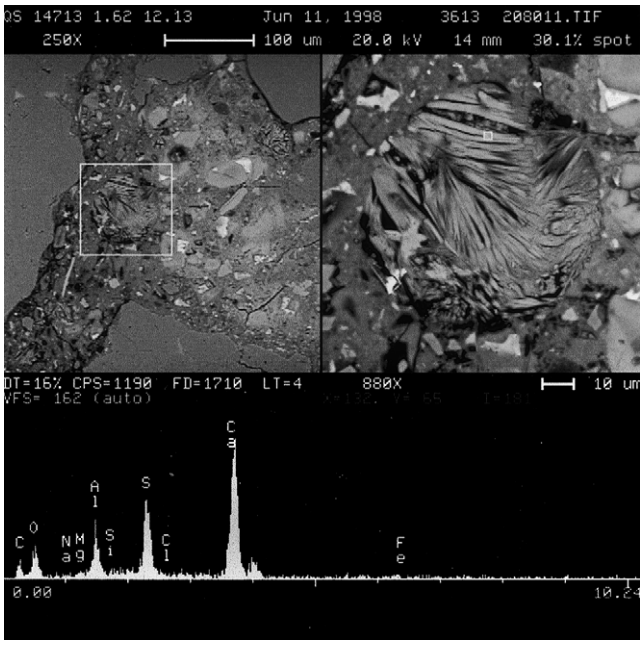

Fig. 16. The EDS spectrum of the second solid filling the air void shown in Fig. 15. The spectrum and the morphology of this solid shows it to be ettringite.

region shown in Fig. 14 is the result of brucite precipitation is also typical of magnesium sulfate attack [10,15].

As in the w/c 0.45 concrete prepared with Type V cement, both ettringite and thaumasite are observed. Fig. 15 shows an air void filled with materials that exhibit similar, but not identical, morphologies. The EDS spectrum for the region shown in Fig. 15 indicates the presence of thaumasite. Alternatively, the spectrum for the region of this same air void shown in Fig. 16 indicates the presence of ettringite. There is no indication of

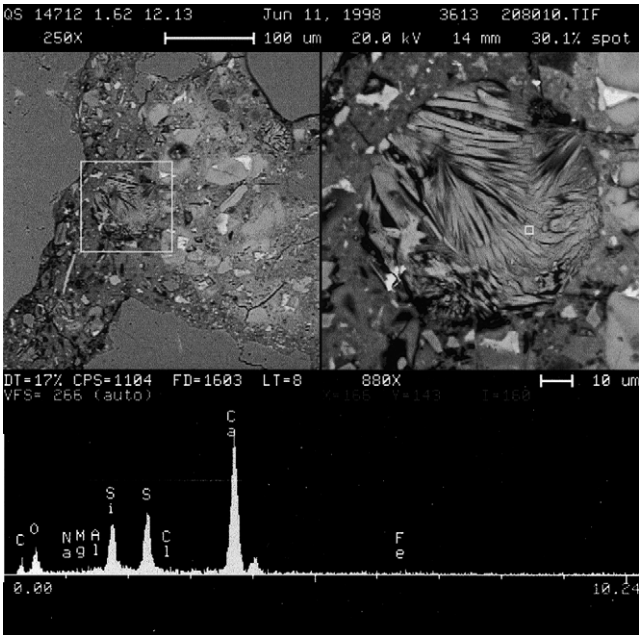

Fig. 15. An air void filled with two solids having similar, but not identical, morphologies. The EDS spectrum from the region shown indicates it to be thaumasite.

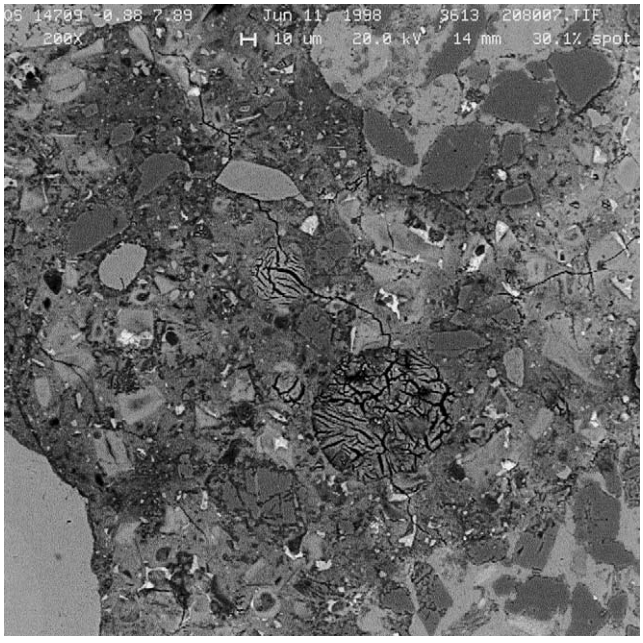

Fig. 17. A region in which the pores and voids in cement paste have been completely filled. Cracks have propagated between air voids.

Al in the thaumasite spectrum or of Si in the ettringite spectrum. While the existence of solid solubility between ettringite and thaumasite has been established [16], the present data suggest the absence of a solid solution between the two in this instance. However, a similar analysis of an adjacent air void indicates a region with a spectrum containing both Al and Si. Thus, while that observation may be regarded as evidence to suggest solid solubility, the morphological differences between ettringite and thaumasite are also evident in this air void. These findings indicate an intimate mixture of thaumasite and ettringite can result in EDS spectra containing both Si and Al peaks. Thus, in this instance the association between Al and Si peaks appear to have resulted from a physical mixture of the two rather than from a solid solution between them.

Fig. 17 shows a feature typical of those observed in these concretes. Two ettringite-filled air voids can be seen in this micrograph. These are connected by a crack traversing this region extending from upper left to lower right. ASTM Standard Practice C-856 [17] suggests that the formation of ettringite in air voids of concrete produced from Type II cement is the result of its recrystallization. However, the microstructural evidence illustrated in Fig. 17 indicates this not to be true. Rather, ettringite can deposit in air voids for at least two reasons. One is due to ettringite recrystallization associated with moisture movement through concrete in the absence of an external sulfate source. This is not external sulfate attack. Alternatively, as Fig. 17 illustrates, sulfate attack is capable of forming sufficient ettringite to initially fill air voids and to eventually cause them to act as local centers of tensile stress that lead to crack formation. This phenomenon was observed regardless of whether the concrete was produced using Type II or Type V cement.

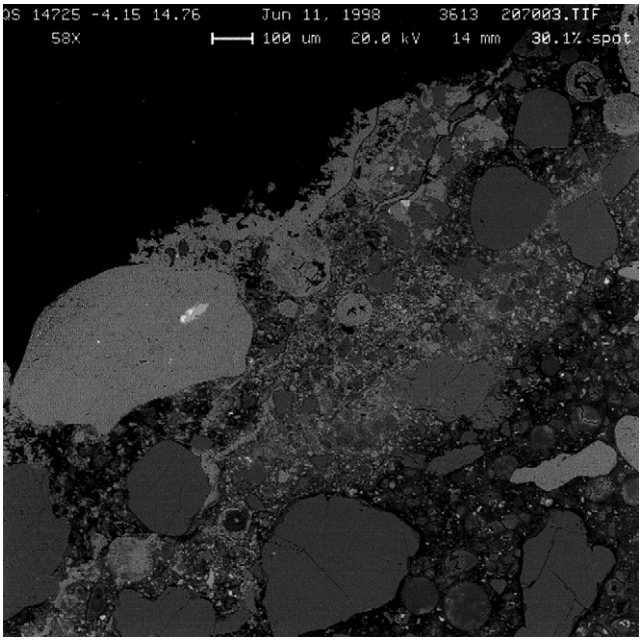

Fig. 18. The near-surface microstructure of a w/c = 0.5 Type II cement concrete after immersion in Na_2SO_4 solution for 22 years. A carbonated layer approximately 700 μm thick can be observed. Completely filled air voids can be observed.

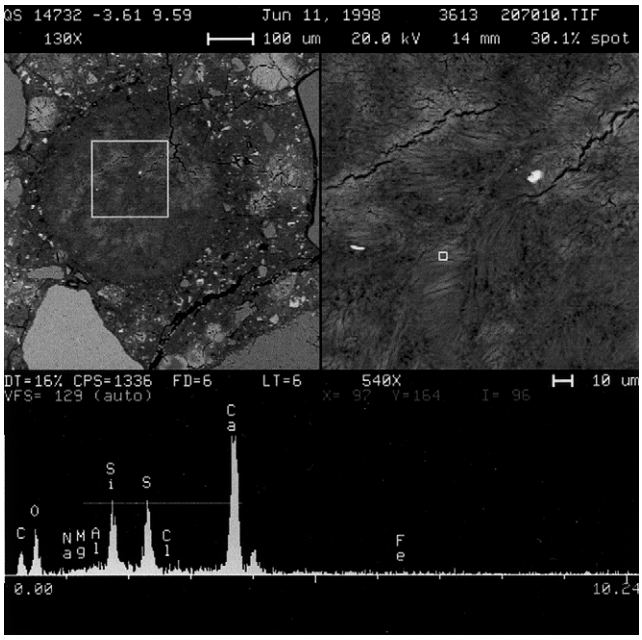

Fig. 19. A filled air void in which the thaumasite crystallites are so tightly packed that their fibrous morphology is not readily apparent in some regions.

3.4. Concrete containing Type II cement, $w/c = 0.5$, Na_2SO_4 solution

The most aggressively attacked concrete of the four studied was that prepared using a Type II cement, at a w/c of 0.50 and immersed in Na_2SO_4 solution. Ettringite formation was observed throughout the sample analyzed. Fig. 18 shows the near-surface region of this concrete. A distinct zone of $CaCO_3$ can be observed. The microstructural features observed in Fig. 18 can be compared with those in Fig. 2. The air voids in this zone are filled with $CaCO_3$. Filled air voids can also be observed immediately below this zone. One such void is shown in Fig. 19 to contain thaumasite that has filled this space to a high degree. In addition to thaumasite, ettringite can be observed in air voids and throughout the paste. In some regions gypsum has replaced calcium hydroxide at the paste–aggregate interfaces, Fig. 20; in other regions mixtures of ettringite and thaumasite appear to have accumulated at the paste–aggregate

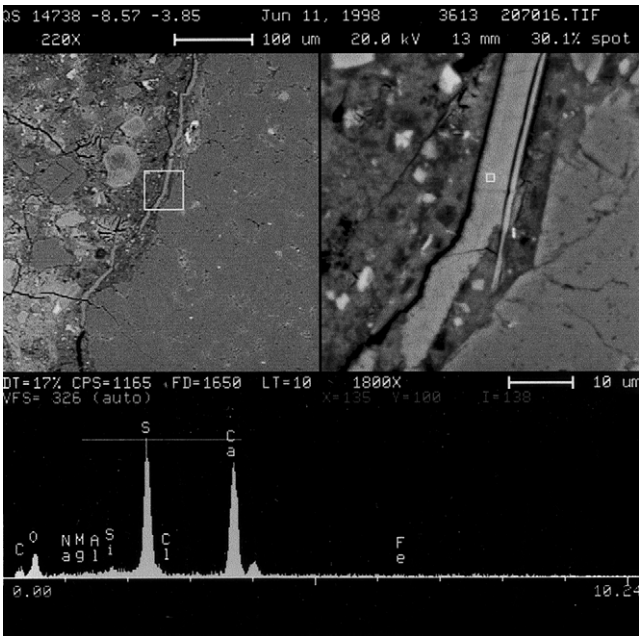

Fig. 20. The paste–aggregate region where $Ca(OH)_2$ has been completely replaced by gypsum.

Table 1
Depth of sulfate attack after 21 years exposure

Cement type	w/c ratio	Attacking species	Depth of attack
V	0.45	$MgSO_4$	7 mm
V	0.45	Na_2SO_4	22 mm
II	0.50	$MgSO_4$	32 mm
II	0.50	Na_2SO_4	Throughout (at least 37.5 mm)

interfaces. Thus, this concrete has undergone extensive microstructural modification.

4. Conclusions

Ettringite has been shown to form in concretes produced with sulfate-resisting cements. Selection of Type V cement was inadequate to confer immunity to sulfate attack and ettringite formed in sufficient quantity to cause the cracking characteristic of sulfate attack. The extent of ettringite formation appears to correlate with the nature of the sulfate-containing species ($MgSO_4$ vs. Na_2SO_4) and with the w/c. Table 1 lists the approximate depths of attack depending on cement type, the nature of the cation associated with the sulfate, and w/c ratio. For example, concretes produced using both cement types were more extensively attacked by immersion in Na_2SO_4 solution than by immersion in $MgSO_4$ solution even though the Mg cation also participated in aggressive reactions. However, Mg-containing reaction products formed on and near the surfaces and in doing so reduced surface permeability. This illustrates the importance of that permeability reduction in controlling sulfate attack. Although Powers [18] demonstrated only a modest increase in the permeability of cement paste in increasing the w/c ratio from 0.45 to 0.5, the present microstructural data illustrate the depth of sulfate attack to increase significantly over this range of w/c ratios.

Thaumasite formation was extensive regardless of cement type, w/c or sulfate source. Significantly, although thaumasite formation is frequently regarded as a low-temperature phenomenon, it was observed in specimens stored at ambient conditions. In general, the depth to which thaumasite was observed was less than that for ettringite. This relationship would be expected under two circumstances. Because thaumasite formation requires the ingress of sufficient CO_2 to decompose C–S–H, it can be anticipated to initiate after ettringite formation has reached a substantial completion in a particular region. This suggests ettringite formation to be complete in regions showing mixtures of ettringite and thaumasite. Alternatively, if thaumasite formation is associated with the end-state of concrete, it will persist after the ettringite has decomposed. In this situation sulfate and aluminate will be liberated and may form additional ettringite in regions where it is stable.

Acknowledgements

The authors gratefully acknowledge April (Doerr) Snyder and Traci Lersch of the RJ Lee Group for their assistance in the acquisition of the microstructures shown in this paper. Also, the authors would like to acknowledge John Emery of John Emery Geotechnical Engineering Ltd. for allowing one of us (Hooton) to maintain these concrete specimens.

References

[1] Swensen EG, editor. Performance of Concrete. Toronto: Univ of Toronto Press; 1968.
[2] George Verbeck Symposium on Sulfate Resistance of Concrete, ACI SP-77, 1982.
[3] Mehta PK. Sulfate attack on concrete – A critical review. In: Skalny JP, editor. Materials science of concrete. Westerville: American Ceramic Society; 1992. p. 104–30.
[4] Marchand J, Skalny JP, editors. Materials science of concrete: sulfate attack mechanisms. Westerville: American Ceramic Society; 1999. p. 73–98.
[5] ASTM Designation C-150. Standard specification for Portland cement, 2000 Annual book of ASTM standards, vol. 4.01, 2001.
[6] Verbeck GJ. Field and laboratory studies of the sulphate resistance of concrete. In: Performance of concrete. Toronto: University of Toronto Press; 1968. p. 113–24.
[7] Erlin B, Stark DC. Identification and occurrence of thaumasite in concrete. Highway Res Rec 1965;113:108–13.

[8] Van Aardt JHF, Visser S. Thaumasite formation: A cause of deterioration of portland cement and related substances in the presence of sulphate. Cem Concr Res 1975;5:225–32.
[9] Crammond NJ. Thaumasite in failed cement mortars and renders from exposed brickwork. Cem Concr Res 1985;15:1039–50.
[10] Brown PW, Doerr A. Chemical changes in concrete due to the ingress of aggressive species. Cem Concr Res 2000;30:411–8.
[11] Hooton RD, Emery JJ. Sulfate resistance of a canadian slag cement. ACI Mater J 1990;87(6):547–55.
[12] Bonen D, Cohen MD. Magnesium sulfate attack on portland cement paste – I. Microstructural analysis. Cem Concr Res 1992;22:169–80.
[13] Bonen D, Cohen MD. Magnesium sulfate attack on portland cement paste – II. Chemical and mineralogical analysis. Cem Concr Res 1992;22:697–708.
[14] Gollop RS, Taylor HFW. Microstructural and microanalytical studies of sulfate attack. V. Comparison of different slag blends. Cem Concr Res 1996;26:1029–44.
[15] Brown PW, Badger S. The distributions of bound sulfates and chlorides in concrete subjected to mixed NaCl, $MgSO_4$, Na_2SO_4 attack. Cem Concr Res 2000;30:1535–42.
[16] Barnett SJ, Halliwell MA, Crammond NJ, Adam CD, Jackson ARW. Study of thaumasite and ettringite phases formed in sulfate/blast furnace slag slurries using XRD full pattern fitting, Cem Concr Composites 2002;24:339–346.
[17] ASTM Designation C-856. Standard practice for petrographic examination of hardened concrete, 2000 Annual book of ASTM standards, vol. 4.02, 2001.
[18] Hearn N, Hooton RD, Mills R. Pore structure and permeability. In: ASTM STP, 169C. 1994 [chapter 26].